

Bedform Effect on the Reorganization of Surface and Subsurface Grain Size Distribution in Gravel Bedded Channels

Arvind SINGH¹, Michele GUALA¹, Stefano LANZONI²,
and Efi FOUFOULA-GEORGIU¹

¹St. Anthony Falls Laboratory and National Center for Earth-surface Dynamics,
Department of Civil Engineering, University of Minnesota, Minneapolis, USA
e-mail: sing0336@umn.edu

²University of Padova, Department IMAGE, Padova, Italy

Abstract

Quantification of river bedform variability and complexity is important for sediment transport modeling as well as for characterization of river morphology. Alluvial bedforms are shown to exhibit highly non-linear dynamics across a range of scales, affect local bed roughness, and vary with local hydraulic, hydrologic, and geomorphic properties. This paper examines sediment sorting on the crest and trough of gravel bedforms and relates it to bed elevation statistics. The data analysed here are the spatial and temporal series of bed elevation, grain size distribution of surface and subsurface bed materials, and sediment transport rates from flume experiments. We describe surface topography through bedform variability in height and wavelength and multiscale analysis of bed elevations as a function of discharge. We further relate bedform migration to preferential distribution of coarse and fine sediments on the troughs and crests, respectively, measuring directly surface and subsurface grain size distributions, and indirectly the small scale roughness variations as estimated from high resolution topographic scans.

Key words: bedforms, roughness, grain sorting, power spectral density, sediment transport.

1. INTRODUCTION

Bedforms present on the bed surface of a gravel-bed river are highly variable and strongly depend on the local bed shear stress and grain size distribution of bed material (Nordin 1971, Paola and Borgman 1991, Powell 1998, Buffington and Montgomery 1999, Lanzoni 2000, Kleinhans *et al.* 2002, Blom *et al.* 2003, Blom and Parker 2004, van der Mark *et al.* 2008, Singh *et al.* 2011). They evolve as a result of the complex interaction between turbulent flow field, sediment transport and underlying fluvial bed topography (Jerolmack and Mohrig 2005, Best 2005, Venditti *et al.* 2005, Venditti 2007, Singh *et al.* 2010, Singh and Fofoula-Georgiou 2012). Quantification of their formation and evolution is essential towards understanding their interaction with flow turbulence and particle transport, interpretation of sedimentary structure, developing predictive models for sediment transport, river management as well as river habitat dynamics (Simons *et al.* 1965, Nelson *et al.* 1993, 1995, Yarnell *et al.* 2006, ASCE 2002, Best 2005, McElroy and Mohrig 2009, Wilcock 1998, Leclair 2002).

Several studies have focused on characterizing bedform variability using both numerical, theoretical and empirical approaches (Paola and Borgman 1991, Coleman and Melville 1994, Lanzoni and Tubino 1999, Blom *et al.* 2003, Jerolmack and Mohrig 2005, Coleman *et al.* 2006, Van der Mark *et al.* 2008, Singh *et al.* 2011). For example, Jerolmack and Mohrig (2005) developed a nonlinear stochastic surface evolution model which reproduces laboratory observations of evolution of bedforms and their long term dynamical behavior as observed in natural systems. Van der Mark *et al.* (2008) used controlled laboratory and field studies to characterize variability in bedform geometry and suggested that bedform variability can be represented by an exponential function for the coefficient of variation.

For a bed with a wide grain size distribution, as in the case of real rivers, bedform variability results in preferential movement and deposition of sediment causing significant changes in the local bed roughness (see *e.g.*, Lanzoni and Tubino 1999, Blom *et al.* 2003, Blom 2008). Traditionally, to characterize gravel bed roughness, percentiles of the grain size distribution of the surface patches are used (*e.g.*, Nikora *et al.* 1998). However, it has been argued that the roughness characteristics of a bed cannot be only approximated with a single parameter, say d_{84} , since other factors, *e.g.*, particle shape, orientation, structural arrangement of the particles and bedform geometry are also important. More recently, statistical approaches, such as variograms and higher order structure function analysis have been explored, using high resolution surface elevations, as an alternative to describe the bed roughness (see *e.g.*, Butler *et al.* 2001, Nikora and Walsh 2004, Aberle and Nikora 2006).

In gravel bed rivers, to the best of our knowledge, statistical properties of bedform-dominated beds have not been related to the observed grain size distribution, except in the study of Blom *et al.* (2003). Blom *et al.* (2003) related the observed probability density function of the bed elevation, specifically bedform trough elevation, to the vertical sorting within the bedform. More recently, Blom *et al.* (2008) proposed a morphodynamic model which reproduces time evolution of the vertical sorting profile and grain size distribution of bed load transport. In contrast to the bedform-dominated beds, on plane-beds, only recently, a few studies have focused on multiscale statistical characterization of bed elevation fluctuations and their relation to observed grain size distribution (Nikora *et al.* 1998, Butler *et al.* 2001, Aberle and Nikora 2006).

The goal of this study is to understand and quantify how an initial grain size distribution of bed material is redistributed preferentially within the macroscale structures (crest and trough of bedforms) of the bed, both on the surface and in the subsurface layers in bedform-dominated gravel bed rivers. The data analysed are the high resolution spatial and temporal bed elevation series, grain size distribution of surface and subsurface layers, and the sediment transport rates collected in a large-scale experimental channel. Specifically, we relate small-scale roughness due to grain sizes to the large-scale roughness due to bedforms. We also perform multi-scale statistical characterization of bed elevation fluctuations obtained under different flow conditions.

The paper is organized as follows. In Section 2 we briefly describe the experimental setup and the data collected in two laboratory experiments under low and high flow conditions. Section 3 focuses on physical characteristics of bed topography, while Section 4 discusses multiscale statistics of bed elevations. In Section 5, an analysis on grain size distribution is performed whereas the relation between observed grain size distribution and bed elevations of patches of crest and trough is explored in Section 6. Section 7 focusses on discussion of the results obtained whereas Section 8 presents summary and the concluding remarks.

2. EXPERIMENTAL SETUP AND DATA COLLECTED

The experiments reported here were conducted in a large-scale experimental channel, called Main Channel, at the St. Anthony Falls Laboratory, University of Minnesota. These experiments were the follow-up of previous experiments conducted in the spring of 2006 known as StreamLab06 (Singh *et al.* 2012b). The Main Channel is 84 m long, 2.75 m wide, and has a maximum depth of 1.8 m with a maximum discharge capacity of 8000 l/s. Only the first 55 m long upstream reach of the channel was used in these experi-

ments. The sediment was partially recirculated while the water, taken directly from the Mississippi River, was fed to the channel without recirculation.

The channel was filled with a 0.45 m thick layer of sediment, composed of a mixture of gravel and sand with density about 2650 kg/m^3 , with a median particle size diameter $d_{50} = 7.7 \text{ mm}$, and an overall grain size distribution (hereafter GSD) characterized by $d_{16} = 2.2 \text{ mm}$ and $d_{84} = 21.2 \text{ mm}$.

To achieve dynamic equilibrium in transport and slope adjustment for both water surface and sediment bed, a constant water discharge Q was fed into the channel prior to the data collection. This dynamic equilibrium state was evaluated by checking the stability of the 60 min average total sediment flux at the downstream end of the test section. Continuous data collection occurred for about twenty hours after the channel had reached dynamic equilibrium.

The data presented here are the spatial and temporal series of bed elevation, grain size distribution, and the sediment transport rates. The spatial series of bed elevations were collected by a three-axis positionable data acquisition (DAQ) carriage, capable of traversing the entire $55 \times 2.74 \text{ m}$ test reach and positioning probes with an accuracy of 1 mm along all the three

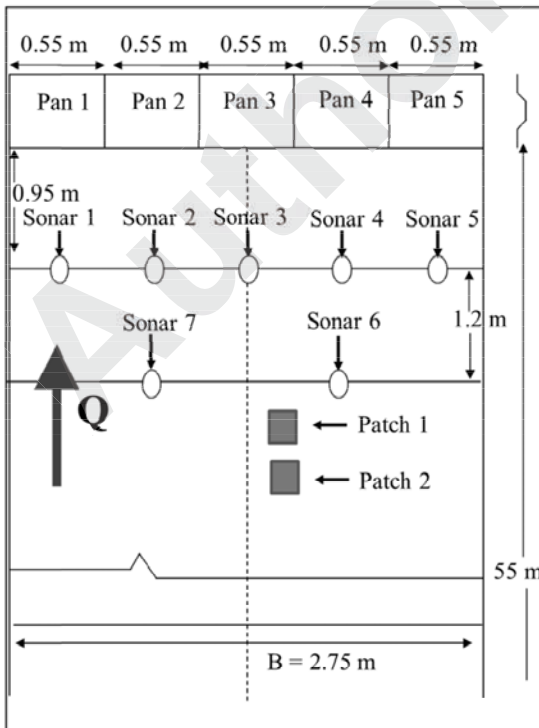


Fig. 1. Schematic of the Main Channel showing the location of sonars used to measure temporal bed elevations, of sediment pans used to monitor sediment transport rates and of the patches considered for sampling of sediment used to determine surface and subsurface grain size distributions. Spatial bed elevations were sampled by laser scanner mounted on a positionable data acquisition carriage that can move along the 55 m long test section. The dashed line represents the centerline of the channel while the direction of the flow is from bottom to the top of the figure.

axes. The sampling resolution of the spatial bed elevation was 1 cm in both streamwise and spanwise direction. The temporal bed elevations were measured through submersible sonar transducers of 2.5 cm diameter, deployed 0.3 m (on average) below the water surface, at the downstream end of the investigated reach (Fig. 1). The sampling interval of temporal bed elevation measurements was 5 s with a vertical precision of 1 mm.

Bedload traps located at the downstream end of the test reach, consisting of 5 weighing pans of equal size that spanned the width of the channel, were used for measuring sediment transport rates (Fig. 1). The weight of bedload sediment falling into the weigh pans was automatically recorded every 1.1 s. To remove the negative, unphysical values that sometimes appeared in the record of sediment transport rate sequence, a moving average window of 2 min was used (see Singh *et al.* 2009). A typical series of 2 min averaged sediment transport rates is shown in Fig. 2 for the discharges of 1500 l/s (Fig. 2a) and 2800 l/s (Fig. 2b). After the weigh pans filled with a maximum of 40 kg of sediment, their base tipped to release the sediment and reset the weigh pan. The released sediment was re-circulated and returned back into the channel at the upstream end of the 55 m test reach, to maintain equilibrium conditions through a closed system.

In order to study the GSD of surface and subsurface composition of the bed material, the channel was drained at the end of each experiment and

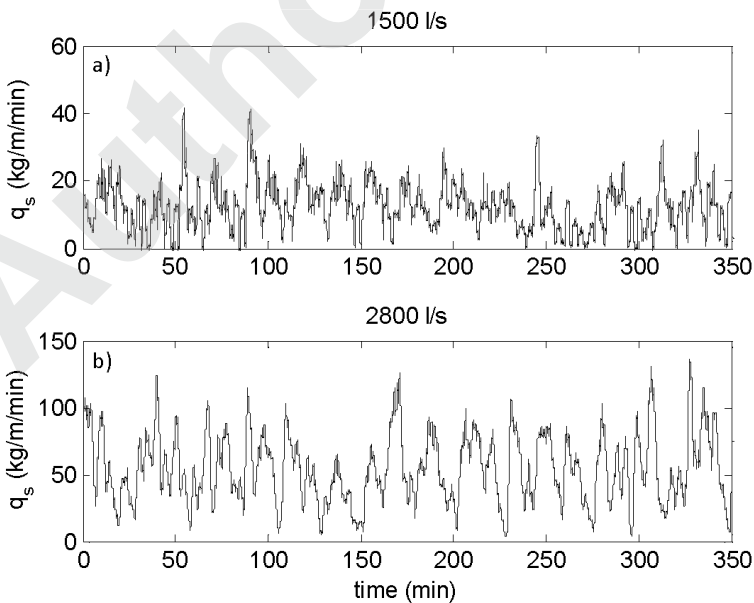


Fig. 2. Two minutes averaged sediment transport rates for the discharges of: (a) 1500 and (b) 2800 l/s.

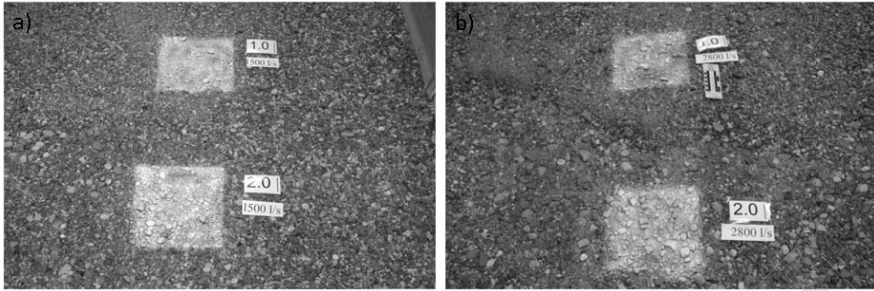


Fig. 3. Photographs of the patches of bed surfaces obtained at the end of the experiments carried out with discharges of: (a) 1500 and (b) 2800 l/s. Note that marks 1 and 2 are located in the correspondence of bedform crests and troughs, respectively.

surface layers of 30×30 cm patch size were painted, after identifying the patch location on the bedform crest and trough (Fig. 1). The surface layers of these patches were carefully extracted for determining the surface GSD; a 10 cm deep layer of bed material was then excavated in order to determine the subsurface GSD. Figure 3 shows the marked patches on the crest and the trough of bedforms observed at the end of runs carried out for discharges of 1500 (Fig. 3a) and 2800 l/s (Fig. 3b).

Although measurements were taken over a range of discharges corresponding to different bed shear stresses, here, for the sake of brevity we consider only the data collected at discharges of 1500 l/s (low flow) and 2800 l/s (high flow), corresponding to Shields stress of 0.049 and 0.099, respectively (for details about the hydraulic conditions see Table 1). The critical Shields stress (τ_c^*), determined on the basis of the median grain size of the mixture $d_{50} = 7.7$ mm, was assumed to be 0.03 as suggested by Buffington and Montgomery (1997) and references therein. The aspect ratio (channel width/flow depth) corresponding to the investigated flows were 6.4 and 4.3 for the discharges of 1500 and 2800 l/s, respectively.

Table 1
Hydraulic conditions and statistics of spatial bed elevation

Q [l/s]	D [m]	V [m/s]	S_w	h_R [m]	τ_b^*	std($h(x)$) [mm]
1500	0.43	1.27	0.0019	0.33	0.049	16.19
2800	0.64	1.59	0.0029	0.44	0.099	39.28

Explanations: Q – water discharge, D – average flow depth along test reach, V – average flow velocity, S_w – water surface slope, h_R – hydraulic radius, τ_b^* – dimensionless shields stress (computed using hydraulic radius), std($h(x)$) – standard deviation of spatial bed elevation.

3. BED TOPOGRAPHY

3.1 Physical characteristics

The bedforms formed within the channel consisted mainly of bedload sheets at the low discharge (1500 l/s) and of three-dimensional dunes at the high discharge (2800 l/s). Figure 4 shows the bed elevation profile at the flume centerline for the two discharges here considered. It can be seen that the low flow run (Fig. 4a) produced a channel bed with only limited topographic variation, *i.e.*, without obvious large-scale bed structures: the standard deviation of the detrended (linear trend removed) bed elevation being 16.19 mm as compared to a d_{50} grain size of 7.7 mm. Conversely, the high flow run (Fig. 4b) generated substantial bed variability (std. dev. = 39.28 mm) at large scale in the form of dunes, with intermediate to grain-scale fluctuations superimposed on them (Table 1). In particular, the standard deviation of the detrended bed elevation roughly doubled (from 16.19 to 39.28 mm) by increasing the discharge from 1500 to 2800 l/s, suggesting that bed fluctuations are more variable at higher discharge.

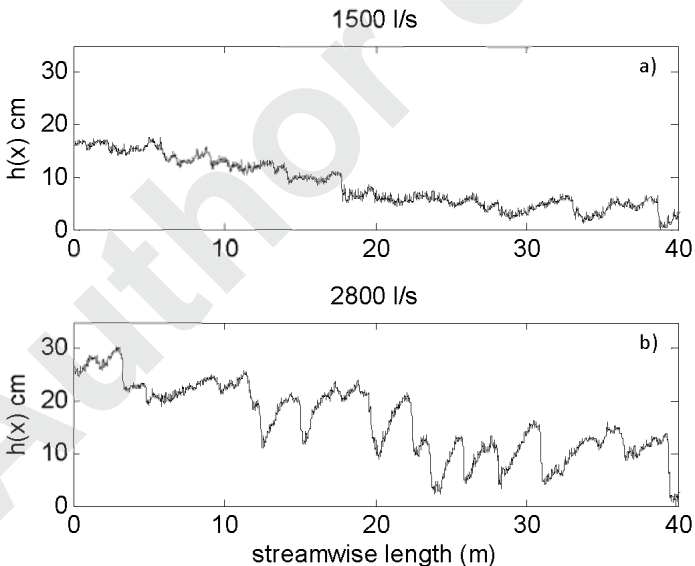


Fig. 4. Longitudinal transects of the spatial bed elevation sampled at the channel centerline at a resolution of 10 mm after the end of the experiment for the discharges of: (a) 1500 and (b) 2800 l/s. Note that the zero bed elevation ($h(x) = 0$) does not correspond to the base of the flume but corresponds to the lowest bed elevation (reference point) below which no elevation fluctuations were observed for a given discharge. A linear trend was removed from the above shown transects to compute the standard deviation of detrended bed elevation (see the statistics of detrended bed elevation in Table 1).

3.2 Bedform extraction

The geometric characteristics of bedforms were extracted from the longitudinal spatial transects of bed elevation, obtained at distances of 0.5 m apart across the width of the flume, using the methodology described in Singh *et al.* (2011). From these transects, first, the high-wavenumber fluctuations (wavenumber $> 10^{-2} \text{ mm}^{-1}$, corresponding to wavelengths smaller than 10 cm) induced by small scale bedforms or grain-scale variations were filtered out using the Fourier transform of the signal and then the signal was reconstructed with all wavenumbers $< 10^{-2} \text{ mm}^{-1}$ (note that the filtered wavenumbers correspond to the high wavenumbers in the power spectral density of bed elevation, discussed later in Section 4, where the transition in the slope of the power spectral density occurs). Then, after determining the local maxima and minima in the filtered signal, the differences between consecutive minima and maxima were computed. Finally, the bedform heights above a certain threshold (threshold = $2d_{50}$) were extracted. Figure 5 shows the probability density function (hereafter pdf) of the extracted bedform heights for the discharges of 1500 (Fig. 5a) and 2800 l/s (Fig. 5b), whereas Fig. 6 shows the corresponding pdfs of bedform lengths for the discharge of 1500 (Fig. 6a) and 2800 l/s (Fig. 6b). The statistics of the extracted bedform heights and lengths are summarized in Table 2 which indicates that the mean and the standard deviation of bedform heights increases with increasing discharge, while an opposite behaviour is exhibited by bedform lengths. A similar trend is followed by the coefficient of variation, CV (standard deviation/mean), which shows that with increasing discharge the CV for the bedform height increases, suggesting a wider range of bedform heights at higher

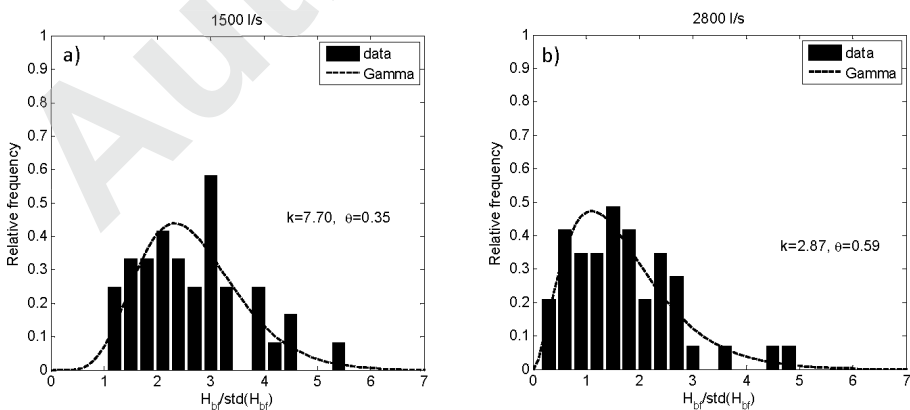


Fig. 5. Probability density function of the normalized bedform heights for the discharges of: (a) 1500, and (b) 2800 l/s. The dotted curve shows the fitted Gamma distribution with k as the shape parameter and θ as the scale parameter.

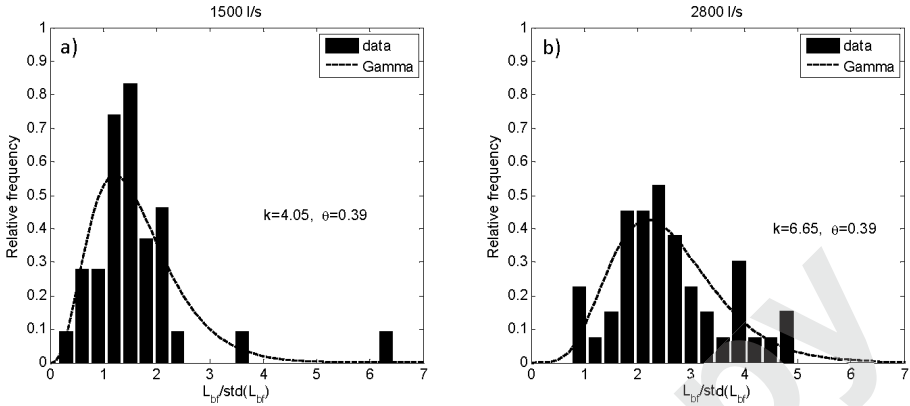


Fig. 6. Probability density function of the normalized bedform lengths for the discharges of: (a) 1500 and (b) 2800 l/s. The dotted curve shows the fitted Gamma distribution with k as the shape parameter and θ as the scale parameter.

Table 2

Bedform statistics extracted from spatial and temporal bed elevations

Q [l/s]	Spatial bed elevation						Temporal bed elevation			
	$\overline{\langle H_{bf} \rangle}$ [mm]	$\text{std}(H_{bf})$ [mm]	CV (H_{bf})	$\overline{\langle L_{bf} \rangle}$ [m]	$\text{std}(L_{bf})$ [m]	CV (L_{bf})	AR	$\overline{\langle H_{bf} \rangle}$ [mm]	$\text{std}(H_{bf})$ [mm]	CV (H_{bf})
1500	32.6	12.2	0.37	3.92	2.43	0.62	120	33.8	9.8	0.29
2800	74.5	44.0	0.59	3.29	1.28	0.38	44	82.3	27.9	0.34

Explanations: $\overline{\langle H_{bf} \rangle}$, $\text{std}(H_{bf})$ – mean and standard deviation of bedform height obtained from the ensemble of bedform heights extracted from different transects of spatial bed elevations measured at the end of a run and from different probe locations from temporal bed elevations; $\overline{\langle L_{bf} \rangle}$, $\text{std}(L_{bf})$ – mean and standard deviation of bedform length obtained from the ensemble of bedform lengths extracted from different transects of spatial bed elevations measured at the end of a run; CV – coefficient of variation of bedform height and bedform length, AR – aspect ratio ($= \overline{\langle L_{bf} \rangle} / \overline{\langle H_{bf} \rangle}$).

discharge, whereas the CV for the bedform length decreases suggesting a narrower range of bedforms lengths at higher discharge. Similarly, the ratio of mean bedform length L_{bf} to mean bedform height H_{bf} (aspect ratio) decreases with increasing discharge (Table 2), *i.e.*, with increasing bedform height bedform length decreases.

Previous literature has suggested that bedform heights and lengths can be represented with a Gamma distribution (*e.g.*, van der Mark *et al.* 2008 and

references therein). The pdf of a Gamma distributed random variable x can be defined as

$$f(x, k, \theta) = \frac{1}{\theta^k \Gamma(k)} x^{k-1} e^{-\frac{x}{\theta}}, \quad (1)$$

where k is the shape parameter and θ is the scale parameter. Gamma distributions were fitted here to the normalized bedform height and length and are shown in Figs. 5 and 6 for reference. These fitted distributions were tested for goodness of fit using the chi square test and the null hypothesis of data coming from Gamma distribution was accepted with a p -value ranging from 0.06 to 0.83. The estimated parameters of the fitted Gamma distribution (estimated using maximum likelihood estimation and shown in Figs. 5 and 6) suggest that both the shape parameter, k , and scale parameter, θ , change with increasing discharge (k decreases while θ increases) for the bedform heights, whereas for the bedform lengths k increases while θ remains constant. Similar results for the bedform heights were obtained from the temporal series of bed elevations (Table 2), as already partially noted by Singh and Foufoula-Georgiou (2012) and Singh *et al.* (2012a).

4. MULTISCALE STATISTICS OF BED TOPOGRAPHY

River bed topography and its evolution are found to exhibit variability across a range of scales. One common way to characterize this variability is via plotting the power spectral density (hereafter PSD). For a discrete signal $F(x)$, the PSD can be defined as

$$S(\omega) = \left| \frac{1}{\sqrt{2\pi}} \sum_{-\infty}^{\infty} F(x) e^{-i\omega x} \right|^2 = \frac{\hat{F}(\omega) \hat{F}^*(\omega)}{2\pi}, \quad (2)$$

where $\hat{F}(\omega)$ is the discrete Fourier transform of $F(x)$, $\hat{F}^*(\omega)$ is its complex conjugate and ω is the wavenumber. Here we place special emphasis on identifying spectral scaling ranges, *i.e.*, ranges of scales over which log-log linearity is observed in the power spectral density.

Figure 7 shows the PSD of the spatial bed elevation series for the discharges of 1500 (lower spectrum) and 2800 l/s (upper spectrum). It can be seen that the PSDs follow a power law-decay with a slope ~ 1.7 for the discharge of 1500 l/s and ~ 2.3 for the discharge of 2800 l/s, suggesting the presence of statistical scaling in the bed elevation series. Note that these slopes were estimated for the same range of scales (see Table 3). The largest length scale of bedform observed from these PSDs is of the order of 10 m for both discharges. Similar results of increasing slope of PSDs with increasing discharge are observed from the analysis of temporal bed elevation series. For example, the slope of the PSD for the discharge of 1500 l/s is ~ 1.9 ,

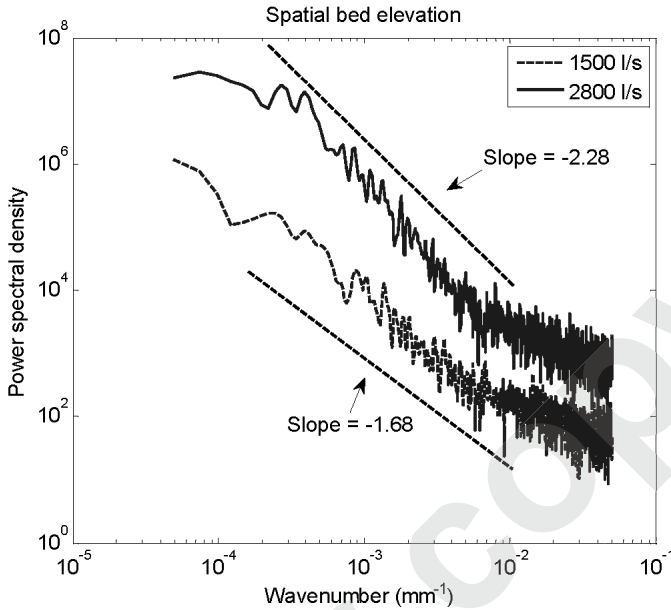


Fig. 7. Power spectral density of spatial bed elevation for the discharge of 1500 (lower spectrum: broken line) and 2800 l/s (upper spectrum: solid line). Note that the spectrum at higher discharge (2800 l/s) is displaced vertically by one order of magnitude.

Table 3

Multiscale statistics of bed elevations

Q [l/s]	Spatial bed elevation					Temporal bed elevation				
	Spectral slope	Spectral scaling range	Multi-fractal parameters		Multi-fractal scaling range	Spectral slope	Spectral scaling range	Multi-fractal parameters		Multi-fractal scaling range
			c_1	c_2				c_1	c_2	
1500	1.68	8 cm – 5 m	0.43	0.05	2 cm – 1.5 m	1.87	15 s – 55 min	0.48	0.09	0.5–8 min
2800	2.28	8 cm – 5 m	0.69	0.10	2 cm – 1.4 m	2.18	20 s – 25 min	0.55	0.13	0.5–7 min

whereas for 2800 l/s it is about 2.2. The increase of spectral slope (temporal PSD) with increasing discharge, along with the reduction in scaling regime (Table 3), suggests that the bedforms of comparable energy (height) move faster at higher discharge, as expected.

It is important to note that the PSD characterizes how the second order moment (variance) in the signal changes with scale/frequency and, as such, it

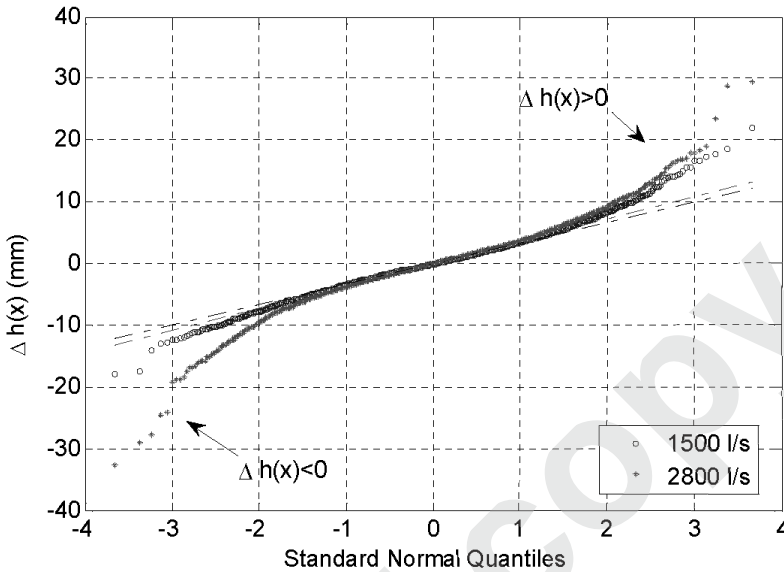


Fig. 8. Quantile-quantile plots of bed elevation increments for the discharges of 1500 and 2800 l/s. The dash lines in the qq-plots represent the Gaussian pdfs. Note that tails of the pdf at higher discharge are thicker than tails at lower discharge.

fully characterizes only a Gaussian pdf over scales (Singh *et al.* 2011). Figure 8 shows the quantile-quantile plots (qq-plot) of $\Delta h(x)$, the bed elevation increments, ($\Delta h(x) = h(x + \Delta x) - h(x)$), where Δx is the resolution of the measurement, *i.e.*, 10 mm) for the investigated discharges. Negative increments of the bed elevation series, $\Delta h(x) < 0$, correspond to depositional events (*i.e.*, an increase of elevation at the point of measurement during an interval Δx) whereas positive values, $\Delta h(x) > 0$, to erosional events. The qq-plots of bed elevation increments reported in Fig. 8 show significant deviation from the Gaussian distribution (dashed lines).

As a consequence, it is important to test for scaling in higher order statistical moments. For this, a higher-order structure function analysis which quantifies the manner in which higher order statistical moments of the local fluctuations in the bed elevation series change with scale was performed. In particular, a statistical analysis was performed on the differences (or increments) of the bed elevation time series $h(x)$ at different scales a , denoted by $\Delta h(x, a)$, and defined as

$$\Delta h(x, a) = h(x + a) - h(x) , \quad (3)$$

where x is the length and a is the scale. The q th order statistical moment estimates of the absolute values of the increments at scale a , $M(q, a)$, are defined as

$$M(q, a) = \frac{1}{N} \sum_1^N |h(x, a)|^q, \quad (4)$$

where N is the number of data points of the series (increments) at scale a . As an extension to second order (spectral) scaling, higher order statistical scaling, or scale-invariance, requires $M(q, a)$ to be a power law function of the scale a , that is

$$M(q, a) \sim a^{\tau(q)}, \quad (5)$$

where $\tau(q)$ is called the scaling exponent function. The most basic form of scaling, known as simple scaling or mono-scaling, occurs when the scaling exponents are a linear function of the moment order, *i.e.*, when $\tau(q) = Hq$. In this case, the single parameter H , known as the Hurst exponent, describes how the whole pdf changes over scales. If $\tau(q)$ is a nonlinear function of q , more than one parameter is required to describe the behavior of the pdf changes over scale and the investigated series is called multi-fractal (Castaing *et al.* 1990, Venugopal *et al.* 2006, Singh *et al.* 2009). The simplest, but not the unique, way to parameterize the nonlinear dependence of $\tau(q)$ on q is via a quadratic approximation defined as $\tau(q) = c_1q - c_2q^2/2$, where c_1 and c_2 are the coefficient of roughness and the coefficient of intermittency, respectively. The parameter c_1 is a measure of the average “roughness” of the series whereas the parameter c_2 gives a measure of the inhomogeneous arrangement of the local fluctuations in the series. The reader is referred to Singh *et al.* (2011) for more details about the structure function analysis.

Figure 9 shows the $\tau(q)$ curves computed from the slopes of the log-log plots of the moments $M(q, a)$ (not shown here for brevity) within the scaling range for the bed elevations at the discharges of 1500 and 2800 l/s, respectively (see Table 3). It can be seen from Fig. 9 that the $\tau(q)$ has a nonlinear dependence on q , which is an indication of the presence of multi-fractality. A summary of the computed multifractal parameters c_1 and c_2 along with the scaling ranges for both the discharges of 1500 and 2800 l/s can be seen in Table 3, along with the multiscale statistics of temporal bed elevation. It is interesting to note that both the roughness coefficient c_1 and the intermittency coefficient c_2 increase with increasing discharge.

The increase of c_2 with increasing discharge suggests a faster rate of change of the pdf's shape across a range of scales (statistical interpretation) and a more inhomogeneous arrangement of abrupt bed elevation fluctuations over space (geometrical interpretation), whereas the increase of roughness parameter c_1 with increasing discharge suggests that bed elevation fluctuations are smoother overall at higher discharge than at lower discharge. Note that the “smoothness” in the signal at higher discharge is associated with the higher Hurst exponent, whereas the abruptness of local, very infrequent fluc-

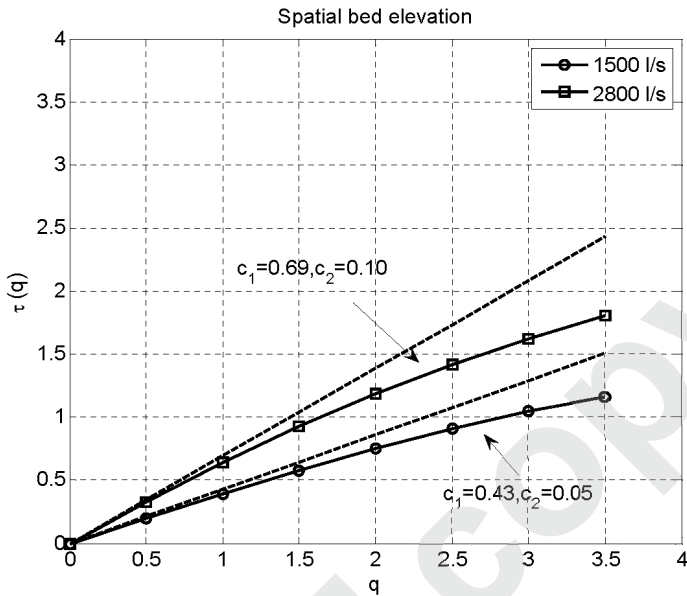


Fig. 9. Scaling exponents $\tau(q)$ estimated from the log-log linear regressions within the scaling regions of statistical moments of spatial bed elevation for discharges of 1500 l/s (bottom curve) and 2800 l/s (top curve). Notice the deviation of $\tau(q)$ from the linear line establishing the presence of multifractality.

tuations is not captured by H . This property is captured with the intermittency parameter c_2 which is higher for higher discharge, indicating that sharp elevation increments due to the passing of steep bedforms or sub-bedforms facies are not homogeneously arranged in the signal (partly due to the fact that bedforms of a wide range of sizes are present at high discharge). Also note that in case of a mono-fractal ($c_2 = 0$), the shape of pdf of the increments does not change with scales and that the slope of the second moment of the structure functions is related to the slope of the PSD via the relation ($\beta = 2H + 1$), where β is the slope of power spectrum, and H is the Hurst exponent. Similar trends of increasing c_1 and c_2 with increasing discharge are observed from the multiscale analysis of temporal bed elevation (see Table 3).

5. GRAIN SORTING IN BEDFORMS

At the end of each run, bedforms were visually identified on the channel bed surface and their crests and troughs were located (Figs. 1 and 3). Patches with dimension of 30×30 cm were marked on both crest and trough (Fig. 3) and their surface (top layer corresponding to one grain size) and sub-surface

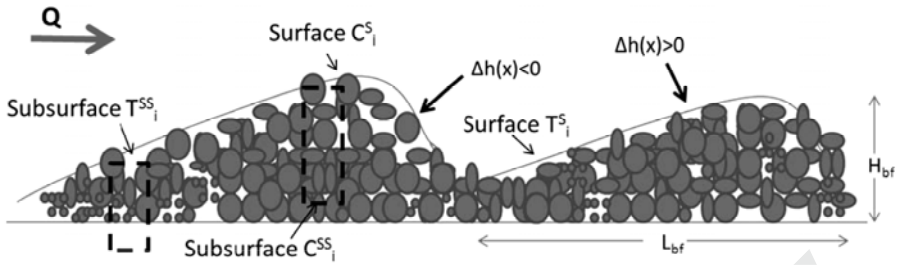


Fig. 10. Typical sketch of investigated bedforms showing the location of patches of surface and subsurface samples, bedform height H_{bf} and bedform length L_{bf} . The subscript i represents patch number, whereas the subscript s and ss represent surface and subsurface, respectively. C and T denote bedform crest and trough, respectively.

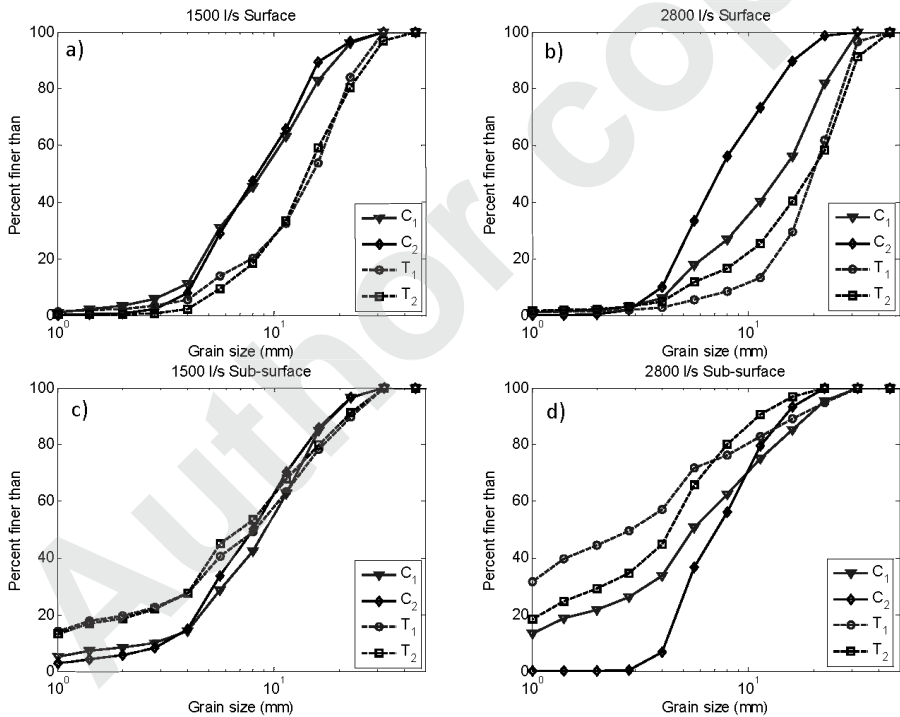


Fig. 11. Grain size distribution obtained from the material sampled at the crest and trough of bedforms for the surface (top panel) and the subsurface (bottom panel) for the discharges of 1500 (left panel) and 2800 l/s (right panel). C_i and T_i ($i = 1, 2$) curves refers to crest and trough samples, respectively.

(10 cm deep material) GSDs were obtained. Figure 10 shows a typical sketch of the observed bedforms and of the sampling locations, whereas Fig. 11 shows the GSDs of both surface (upper panel) and subsurface (bottom

Table 4

Statistics of grain size distribution

Q [l/s]	Patch	Surface				Subsurface			
		d_{16} [mm]	d_{50} [mm]	d_{84} [mm]	Sand [%]	d_{16} [mm]	d_{50} [mm]	d_{84} [mm]	Sand [%]
1500	C1	4.38	8.86	16.54	0.99	4.19	9.25	15.79	5.21
	C2	4.61	8.44	14.94	0.14	2.05	7.97	15.48	2.9
	T1	6.39	15.19	22.69	1.37	1.19	8.15	19.35	14.32
	T2	7.35	14.34	24.67	0.43	1.30	4.61	18.50	13.29
2800	C1	5.35	14.18	23.70	0.99	1.21	5.52	15.49	13.25
	C2	4.41	7.35	14.37	0.11	4.49	7.23	12.85	0.01
	T1	12.12	20.20	28.62	1.13	0.51	2.89	12.23	31.63
	T2	7.67	19.56	29.95	1.50	0.87	4.41	9.22	18.44

panel) samples for the discharges of 1500 (left panel) and 2800 l/s (right panel), while a synthesis of their statistics is reported in Table 4. Below, we characterize the statistics of surface and subsurface GSD as a function of crest and trough for both low and high flow conditions.

5.1 Surface GSD

Figure 11 (top panel) shows the GSDs of the surface patches for the crests and the troughs for the discharges of 1500 (Fig. 11a) and 2800 l/s (Fig. 11b), whereas Table 4 shows the statistics of these patches as a function of discharge. From Fig. 11a it can be seen that for the low discharge the GSDs of the two crests coincide with each other as also do the GSDs of the two troughs. However, for a high discharge the GSDs change their shape considerably (Fig. 11b). The median diameters d_{50} , obtained from different bedforms, for the crests as well as for the troughs are similar for different crests and troughs and increase with increasing discharge (Table 4). Similar trends are observed for d_{16} and d_{84} .

To further compare the GSDs of crests and troughs as a function of discharge, we show in Fig. 12 the average of the crests GSDs ($C = (C1 + C2)/2$) versus the average of the troughs GSDs ($T = (T1 + T2)/2$) for the discharges of 1500 (Fig. 12a) and 2800 l/s (Fig. 12b). Clearly, sorting effects associated with bedforms are enhanced as the bedform amplitude grows and, consequently, the grain size distribution gets wider. For example, the differences between the surface composition at troughs and crests, summarized by the variations in d_{16} , d_{50} , and d_{84} percentiles, are equal to 2.34, 6.11, and 7.93 mm for the discharge of 1500 l/s, whereas they are 5.01, 9.11, and 10.25 mm for 2800 l/s discharge (see Table 5).

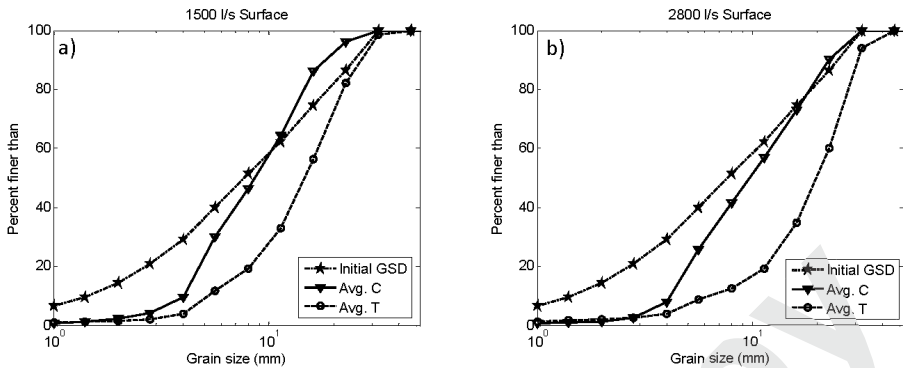


Fig. 12. Comparison of the initial grain size distribution with averaged grain size distribution resulting from surface samples collected at bedform crest and trough for the discharges of (a) 1500 and (b) 2800 l/s.

Table 5

Averaged GSD over bedform crests and troughs

Q [l/s]	Patch	Surface			Subsurface		
		d_{16} [mm]	d_{50} [mm]	d_{84} [mm]	d_{16} [mm]	d_{50} [mm]	d_{84} [mm]
1500	C	4.5	8.65	15.74	3.32	7.69	15.54
	T	6.87	14.76	23.68	1.24	6.37	18.92
2800	C	4.88	10.76	19.03	2.85	6.37	14.17
	T	9.89	19.88	29.98	0.68	3.65	10.73

The averaged GSDs shown in Fig. 12 indicate a departure of the surface grain size distribution with respect to the initial bed composition that, as a consequence of the preferential entrainment of finer particles, is particularly pronounced in bedform troughs. All the representative grain sizes d_{16} , d_{50} , and d_{84} (see Tables 4 and 5) are invariably larger than those characterizing the initial sediment distribution (approximately equal to 2, 8, and 21 mm, respectively) and increase as the discharge increases. An appreciable departure from the shape of the initial GSD is also observed on bedform crests, especially for the lower discharge: the bed composition tends to get coarser owing to a lack in finer fractions (both d_{16} and d_{50} are larger than those of the initial GSD) which compensate the concurrent reduction in coarser fractions (embodied by the decrease of d_{84} from 21 to 15.7 mm). For the higher discharge, this reduction is significantly attenuated ($d_{84} = 19$ mm) while the lack in finer fraction still persists. The recovering, with respect to initial sediment composition, of the upper GSD shape when increasing the discharge is

likely associated with the establishment of a sediment transport condition much closer to equal mobility. On the other hand, the deficiency of finer fractions, that is observed independently of the discharge, is partly related to the winnowing of finer grains from the surface as well as the movement of finer grains into the pores of bed subsurface and partly to the recirculation feeding system, whereby the composition of transported sediment is significantly affected not only by dynamic armor, but also by the intense longitudinal and vertical sorting due to bedform dynamics (Lanzoni 2000).

5.2 Subsurface GSD

The GSDs of the subsurface material sampled at crests and troughs are shown in the bottom panel of Fig. 11 for the discharges of 1500 (Fig. 11c) and 2800 l/s (Fig. 11d) along with their statistics in Table 4, whereas their average GSDs over the bedforms crests and troughs are shown in Fig. 13 for the discharges of 1500 (Fig. 13a) and 2800 l/s (Fig. 13b). The crucial role that bedform migration has on the reworking of the bed and, hence, on determining the composition of the active layer, is clearly attested by the larger variability of GSD curves as the bedform amplitude increases (*i.e.*, at the higher discharge). Although a significant fining of both crests and troughs material, with respect to the initial bed composition, generally characterizes the subsurface samples, the effects are more pronounced at the higher discharge (Fig. 13). Moreover, the material collected below bedform crests is coarser than that sampled below the troughs (Tables 4 and 5). This coarser material results from the inclusion in the bedform body, as a consequence of bedform migration, of the coarser grains previously entrapped in bedform troughs. The pattern of sorting is less clear at the lower discharge (*i.e.*, for

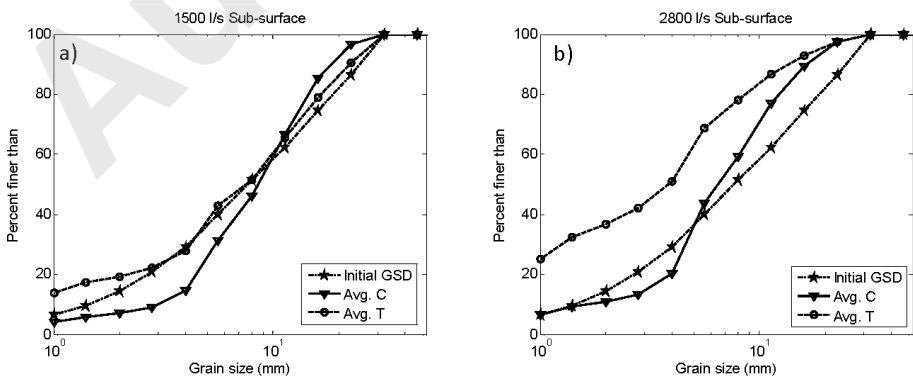


Fig. 13. Comparison of the initial grain size distribution with averaged grain size distribution resulting from subsurface samples collected at bedform crest and trough for the discharges of (a) 1500 and (b) 2800 l/s.

smaller bedforms). In this case, only the values attained by the d_{84} are invariably smaller than those characterizing the initial GSD, while the trends exhibited by the d_{16} and d_{50} are not univocal.

5.3 Surface, subsurface GSD: comparison of quantiles

The upper 10 percentiles of the observed GSDs of the crests for the surface samples, in general, for both the discharges, show finer trend than the initial GSD, whereas troughs show coarser (Fig. 12). For the subsurface, both crests and troughs are finer than the initial GSD for both the discharges (see Fig. 13). A better visual comparison of quantiles of GSDs of crests and troughs as a function of discharge is shown in Fig. 14 for the surface (Fig. 14a) and the subsurface (Fig. 14b) material. Comparing the two crests,

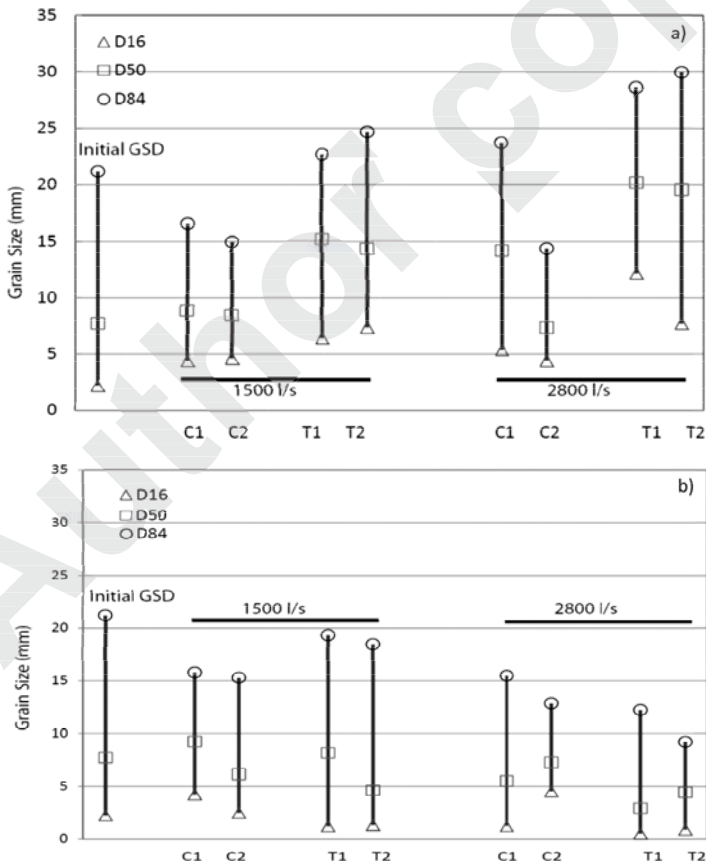


Fig. 14. Comparison of percentiles of GSDs obtained from (a) surface and (b) subsurface sampling at the crests and troughs of the bedform for discharges of 1500 and 2800 l/s.

C1 and C2, within the same discharge for the surface material, it can be seen from Fig. 14a that the crests are more variable at higher discharge. For example, the range of d_{16} to d_{84} is 5.35-23.74 mm for C1, while for C2 it is 4.41-14.73 mm. For the low discharge these ranges are 4.38-16.54 mm and 4.61-14.91 mm for C1 and C2, respectively. The higher variability in crest's grain sorting at higher discharge is due to the fact that at higher discharge bedform heights are more variable (see Table 2). In fact, it is noticed that the bedform heights, extracted from spatial bed elevation series, corresponding to the C1 and C2 for the high discharge are 10.21 and 18.81 cm, while for low discharge they are 4.91 and 5.36 cm, suggesting a higher elevation difference between sampled patches at higher discharge. This difference in C1 and C2 at higher discharge can also be noticed from the difference of mean elevation between C1 and T1, and C2 and T2, which are 3.59 and 9.46 cm, respectively. In contrast to the crests, the troughs do not show significant differences in the sampled patches for both the discharges of 1500 and 2800 l/s (Fig. 14a).

5.4 Integrated GSD

Figure 15 shows the grain size distribution obtained after the integration of GSDs of crests and troughs extracted from surface and subsurface layers for the discharges of 1500 and 2800 l/s. It appears that the integrated GSD recovers most of the grains present in the initial GSD. For example, the d_{50}

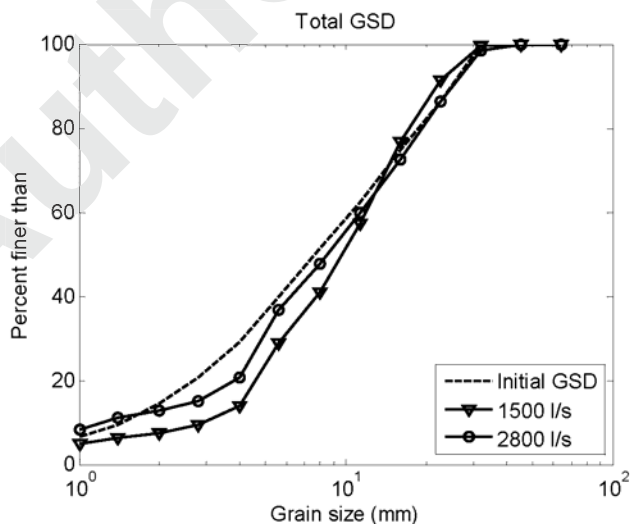


Fig. 15. GSD obtained after the integration of GSDs of crests and troughs belonging to surface and subsurface for the discharges of 1500 and 2800 l/s. Dashed line represents the initial GSD of the bed material.

for the initial GSD and for the integrated GSDs corresponding to the two investigated discharges are 7.7, 9.8, and 8.58 mm, respectively. The small discrepancies emerging from Fig. 15 can be attributed partly to the slope of the bedform stoss side and partly to the distance between the sampled patches. A smaller slope and a closer distance between the patches, associated with smaller bedforms occurring at lower discharge, will produce less distinct differences between the initial GSD and that measured at the end of each experiment.

6. BED ELEVATION STATISTICS OF SAMPLED AND VIRTUAL PATCHES

The bed elevations corresponding to the sediment patches sampled at bedform crests and troughs (Fig. 3) for both low and high discharges were extracted and their statistics were computed. Figure 16 shows the pdfs of the crests and troughs elevation for the discharge of 1500 (Fig. 16a) and 2800 l/s (Fig. 16b), respectively. It can be seen from these figures that while the pdfs of the bed elevation of both crests and troughs are qualitatively similar (*i.e.*, partially overlapping) for the lower discharge, the pdfs observed at the higher discharge are quite different, especially for the crests as also seen in the case of grain size distribution curves (see Figs. 11a-b) (note that here similarity in pdfs is referred to the similarity in the statistics, for, *e.g.*, mean and standard deviation, of the pdfs). The corresponding statistics (mean and standard deviation) reported in Table 6, suggest that bed roughness (measured by the standard deviation of linearly detrended bed elevation) is higher for the troughs than the crests for both discharges. For example, the average standard deviation of the crest and the trough elevations is 3.36 and 4.3 mm, respectively, for the discharge of 1500 l/s, whereas it is 3.34 and 5.97 mm, respectively, for the discharge of 2800 l/s. Moreover, for the higher dis-

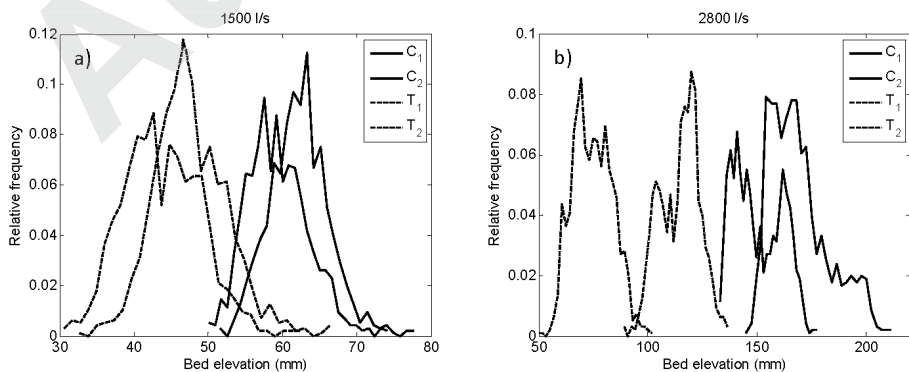


Fig. 16. Probability density functions of bed elevations corresponding to the sampled patches for GSD for the discharges of (a) 1500 and (b) 2800 l/s.

Table 6

Statistics of digital elevation model (DEM) of patches

Q [l/s]	Patch [mm]	Observed patch $h(x,y)$				Virtual patch $h(x,y)$	
		C1	C2	T1	T2	Crest	Trough
1500	Mean	59.33	62.24	43.75	47.64	49.38	39.01
	Std. dev.	3.36	3.36	4.07	4.52	3.44	3.80
2800	Mean	150.41	169.19	114.47	74.53	109.23	84.24
	Std.dev.	4.09	2.58	5.08	6.87	3.49	4.22

charge the crest roughness decreases as the bedform height increases (see the differences in mean elevation for C2 and T2 in Table 6).

The higher discharge is also associated with larger variability in the bed topography, higher complexity and three-dimensionality, essentially related to the wider variety of bedforms that form at this discharge. While the visual selection of crest and trough was still possible, as assessed by the comparative analysis in grain size distribution, its statistical characterization turns out to be more difficult as the bedform topography becomes more complex.

In order to substantiate statistically the results obtained on the analysed patches and provide evidence of sorting effects at the full channel scale, we expand our analysis to virtual patches. As GSD was observed to depend on the specific location of the (sub)surface samples within the bedform (crest or trough), we identify on the digital elevation model (DEM) topography regions with the same size and characteristic location of the crest and trough studied above. The sediment distribution on these virtual patches is obviously unknown but the signature of the coarser grains is expected to survive on the standard deviation of bed elevation computed on each linearly detrended virtual patch, using only DEM data. In other words, the bedform modulation of surface GSD resulting from grain size analysis performed on visually identified patches is expected to hold when comparing small scale roughness over virtual patches. To achieve this goal and further investigate the roughness of sediment patches over crests and troughs, the elevations corresponding to several virtual patches of dimensions 30×30 cm were extracted from the bed profile (Fig. 17). Figure 17 shows the stepwise procedure for extracting virtual patches from the bed elevation profiles for the discharge of 1500 (left column) and 2800 l/s (right column).

Panels (a) and (f) of Fig. 17 show the transects of the bed elevation obtained from the DEM of the bed topography passing through patch 1 for the discharges of 1500 (Fig. 17a) and 2800 l/s (Fig. 17f). Panels (b) and (g) of Fig. 17 show the location of local maxima and local minima superimposed on the filtered (using Fourier transform) bed elevation series;

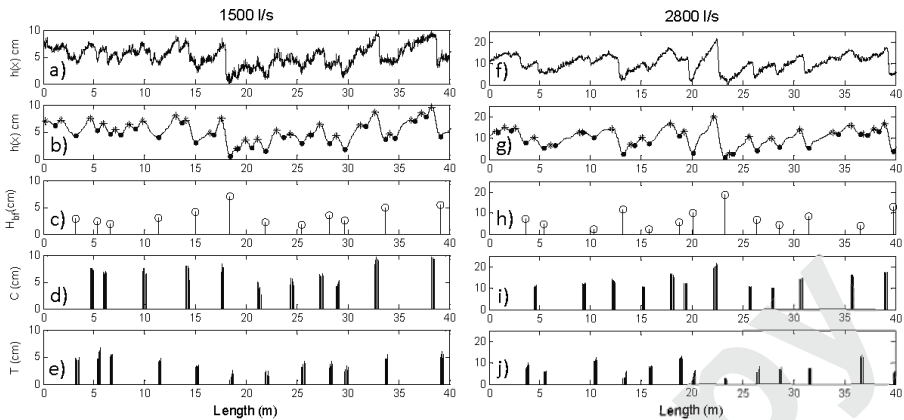


Fig. 17: (a, f) Bed elevation profile, (b, g) location of local maxima (star) and local minima (dot) superimposed on filtered bed elevation using Fourier transform, (c, h) extracted bedform heights after threshold, (d, i) crest elevations, (e, j) trough elevations in mm corresponding to the virtual patch of 30×30 cm. Left column represents 1500 l/s discharge and right column represents 2800 l/s discharge.

Figs. 17c and h show the extracted bedform heights after thresholding (see Singh *et al.* 2011) for details about bedform extraction and thresholding), whereas panels (d), (i) and (e), (j) of Figs. 17 show the crest elevation and the trough elevation, respectively. The statistics (mean and standard deviation) of the extracted virtual patches can be seen in Table 6. As noticed from the sampled patches, the standard deviation (roughness) of the trough elevation is higher than the crest elevation. Blom *et al.* (2003) observed a similar relation, *i.e.*, the trough surface is coarser than the crest surface. They attributed this to the mechanism of winnowing of fines from the trough surface.

7. DISCUSSION

As discussed in the previous sections, the roughness of the gravel bed is usually characterized by the percentiles of the GSD. However, in the presence of bedforms the roughness of the bed significantly changes. In fact, bedforms change the flow conditions, *i.e.*, the flow becomes unsteady and non-uniform locally, especially in shallow channels, a characteristic of gravel channels. Moreover, in the presence of graded sediment, longitudinal and vertical patterns of sorting form as a consequence of the non-uniform bed shear stress distribution along the bedform profile and of the bedform migration. For steady uniform flow and plane bed condition, turbulence (for quantifying sediment transport rates) can be fully characterized by the local bed shear stress (Nelson *et al.* 1995, Schmeeckle and Nelson 2003). However, for

locally non-uniform flow conditions typically occurring in the presence of bedforms, not only the skin friction varies along the bedform surface, but a form drag contribution to the total shear stress also arises (see Wiberg and Nelson (1992) and references therein), which is specifically modulated by the presence of bedforms. Hence in such flows sediment transport modeling generally requires more information than just the total boundary shear stress (Nelson *et al.* 1995, Sumer *et al.* 2003, Singh *et al.* 2012a), since one has to know *a priori* the characteristics of both small scale roughness elements, *i.e.*, grain scale roughness, and large scale roughness due to bedforms.

From the statistics of grain sizes and elevation of sampled patches and from the extracted virtual patches, it was observed that the crests present a typically finer surface grain distribution as compared to troughs (Fig. 14a). Coarser particles then tend to accumulate at bedform troughs under the action of winnowing, forming a coarser matrix that, however, is progressively covered by new material as bedforms migrate downstream. This sorting process is governed by the spatial bed shear stress distribution associated with bedform shape and by the differential entrainment capacity of the flow regions above the troughs (characterized by a lower mean velocity) as compared to the flow regions above the crests. These observations are consistent with the observations of Singh and Fofoula-Georgiou (2012) where it was shown that with increasing discharge the bedform height increases, which creates more space for ejection events in the trough of the bedform. Due to higher ejection events and low velocity in trough of the bedforms, sediment in trough is preferentially entrained, *i.e.*, smaller particles get entrained thus rendering trough surface coarser. As a consequence of the increased variability in bed topography, flow turbulence and grain entrainment with increasing discharge, also the sediment transport is more variable at higher discharge than at lower discharge. For example, in the present experiments, the standard deviation of the 2 min averaged sediment transport rates changes from ~6.8 to ~25.5 kg/m/min as the discharge (and hence bedform height) increases from 1500 to 2800 l/s.

The comparative analysis of surface grain distribution over crests and troughs is not qualitatively affected by the increasing discharge and thus by the sediment transport process. The surface material over the trough is invariably coarser than that found over the crests, the variability of the grain distribution curves tending to increase with bedform size (*i.e.*, discharge). On the other hand, subsurface grain distributions show an opposite trend: the subsurface grain size statistics of the crests (specifically d_{16} and d_{50}) point at a coarser composition with respect to the trough material and the difference increases with increasing discharge (Fig. 14a). A similar trend is observed for d_{84} at the higher discharge, whereas for the low discharge d_{84} of the crests is finer than that over the troughs (see Fig. 14b). While at the low discharge

subsurface distributions differ only in the very fine sediment fraction, for the high discharge the grain size distributions between subsurface layers below crest and trough are observed to vary in the whole range of grain sizes (see Fig. 14b). Why do we observe this strong variability? This could be due to the following reason: the typical bedform height at the low discharge is about 4 cm with a standard deviation of roughly 1 cm. This implies that the subsurface layer (10 cm deep excavation) is statistically below the region intercepted by the moving bedform. It is thus reasonable to expect that subsurface grain size distribution should not exhibit significant differences, regardless of the presence of a crest or trough above them. For larger discharge the mean bedform height is about 7 cm with a standard deviation of 4 cm. Therefore, the subsurface layers are still within the propagating bedforms for the crests. As coarse grain sizes tend to accumulate in the trough with little chance to get entrained or transported away, since in the trough the flow velocity is comparatively low, they get buried by the evolving bedforms. Subsurface grain distributions within a still active layer in terms of transport and sorting mechanisms are in fact expected to show variability in the GSD and thus present differences based on the above topography (crest or trough).

An interesting observation from our experiments is that the troughs at higher discharge for the subsurface material are significantly finer than the initial distribution (compare d_{50} of 2.89, 4.41 mm versus 7.7 mm for T1, T2 and initial distribution, respectively). What creates this re-organization? We suggest that this is due to the variability in bedform height (bedform height corresponding to C1 is about 10 cm whereas bedform height corresponding to C2 is approximately 18 cm). The higher bedform follows a low elevation trough (see the comparison of crests and troughs mean elevation in Table 6): due to this geometry the recirculation zone is bigger (taller) and the flow velocity is lower. As a result, finer material entrained from the following crest and the other upstream bedforms may get settled on the trough and work through the sediment pores to become a part of subsurface, causing the subsurface material to be finer. However, new experiments on flow velocities above gravel bedforms are needed to verify this hypothesis.

It is interesting to note that variability in bed elevation series can be represented as the sum of the small scale roughness (grain scale roughness) and the large scale roughness (bedform scale roughness). It is noticed that for the low discharge, grain scale features contribute about 25% whereas bedform contribute about 75% to the total roughness measured as the standard deviation of the bed elevation series. However, for the higher discharge, the roughness due to bedforms (standard deviation of the bedforms) is much higher than the standard deviation of bed elevation series (see Tables 1, 2, and 6).

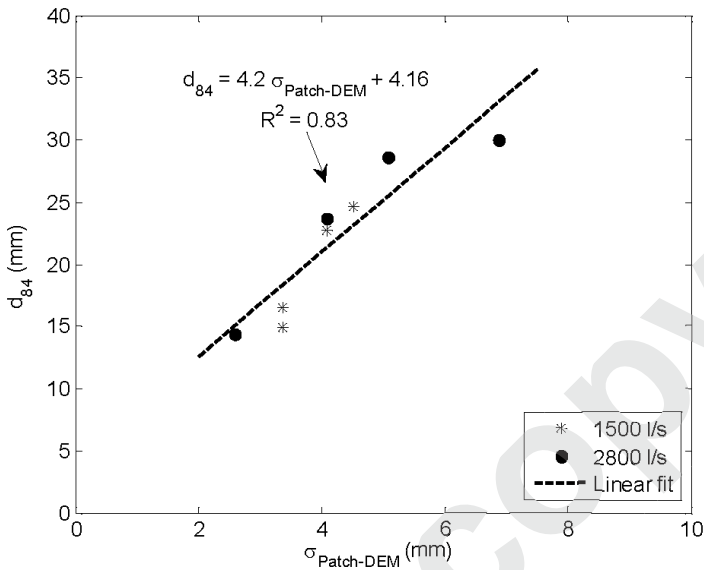


Fig. 18. Predictive relationship between bed elevation standard deviation and d_{84} of grain size distribution of the sampled patches for both the discharges of 1500 and 2800 l/s. Note that the dotted line represents a linear fit.

For modeling accurately the flow field and the sediment transport rates over bedform-dominated river beds, it is required to have *a priori* knowledge of both grain scale roughness and the roughness due to bedforms. Currently available hydrodynamic models, for example, Large Eddy Simulation models, require this information as boundary conditions for improved predictive modelling of flow and sediment transport. The results of this study may provide a better understanding of grain size distribution and roughness parameterization in the presence of bedforms. Figure 18 shows a predictive relation between the standard deviation of the bed elevation and the 84th percentile (d_{84}) of GSD of the sampled patches, whereas Fig. 19 shows the percentage deviation (trough to crest) for the grain sizes (d_{84}) of the sampled patches as a function of percentage deviation in the standard deviation of bed elevation for the same sampled patches, suggesting that local small scale roughness variations measured by the high resolution topography scan can be related to the actual variation in the d_{84} , typically chosen as the parameter controlling frictional roughness effects. A similar behavior, *i.e.*, a high correlation between standard deviation of bed elevation and d_{84} of grain size distribution was observed in Aberle and Nikora (2006), however in that study the bedforms were absent. Figure 20 shows the probability density function of percentage deviation between the crest and the trough for the virtual patches

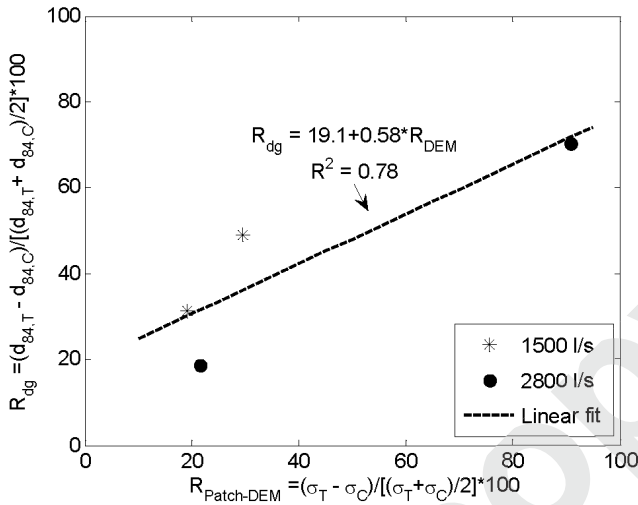


Fig. 19. Percentage deviation (tough to crest) for the grain size (d_{84}) of the sampled patch as a function of percentage deviation of the bed elevation standard deviation of the same sampled patch for the discharges of 1500 and 2800 l/s. Parameters $d_{84,T}$ and $d_{84,C}$ in the y axis represent 84th percentile of GSD of trough and crest patches, respectively, whereas σ_T and σ_C in the x axis represent the standard deviation in the elevation of the sampled patch at trough and crest, respectively.

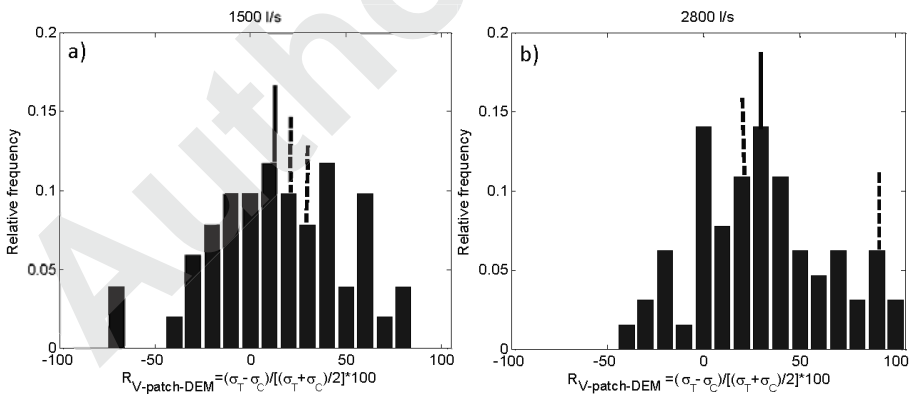


Fig. 20. Probability density functions of percentage deviation in between crests and troughs of virtual patches obtained from the DEM of topography for the discharge of (a) 1500 and (b) 2800 l/s. Note that the dotted line in the pdfs corresponds to the value of percentage deviation ($R_{\text{patch-DEM}}$) obtained for the sampled patches (see Fig. 19) whereas the solid line represents mean of the distribution.

extracted from the bed elevation series for the discharge of 1500 (Fig. 20a) and 2800 l/s (Fig. 20b). The mean percentage deviation obtained for the vir-

tual patches is about 15% for the low discharge, whereas it is approximately 30% for the higher discharge (Table 7). We acknowledge that the percentage deviations for virtual patches are highly variable and also show some negative deviations (Fig. 20). This could be due to the fact that the sorting mechanisms may not always respond to a strong variability in bedform geometry (*e.g.*, in the case of merging or superimposed bedforms).

Table 7

Statistics of percentage deviation between crest and trough
for sampled GSD, sampled patch, and virtual patch

Q [l/s]	R_{dg} [%]	$R_{\text{patch-DEM}}$ (observed patch) [%]	$R_{\text{v-patch-DEM}}$ (virtual patch) [%] (mean)
1500	31.34	19.11	14.77
	49.13	29.44	
2800	18.81	21.59	29.83
	70.31	90.79	

8. SUMMARY AND CONCLUDING REMARKS

This paper investigates the effect of bedform geometry on the particle organization on the surface and subsurface of the crest and trough of the bedform. The data used in this study are the high resolution spatial and temporal bed elevation and grain size distribution of surface and subsurface bed materials of crest and trough of bedforms for low flow and high flow conditions. The experiments were conducted in a large experimental channel at the St. Anthony Falls Laboratory, University of Minnesota. The main results of this study can be stated as follows:

- Statistics of extracted bedform characteristics suggest that the mean and standard deviation of bedform heights increase with increasing discharge, whereas for bedform lengths, the mean and standard deviation decrease with increasing discharge.

- With increasing discharge, bed elevation fluctuations become smoother as suggested by the increasing slope of the power spectral density and the c_1 (multifractality parameter). However, as the variability in bedforms increases, the inhomogeneity in the bed elevation, measured with the intermittency parameter c_2 , increases resulting in the more variable grain size distribution on the crest of the bedform and a stronger sorting effect both in the surface and subsurface layers.

- Bedform migration is observed to induce a preferential grain size distribution (GSD) along the bedform wavelength. In particular, coarser

(finer) sediments were observed to predominantly accumulate in the trough (crest). Sorting effects due to bedform evolution can be interpreted as a scale interaction mechanism where small scale roughness (scaling at the grain scale) is modulated by large scale roughness (scaling at the bedform scale).

□ Sorting effects in the subsurface layers were observed to depend on bedform height distribution, suggesting that sorted surface layers are progressively buried creating layers of coarse and fine materials in the stratigraphy.

□ At high discharge, the statistics of GSD on the crests are more variable than the corresponding ones at low discharge, whereas the GSD at the troughs do not show significant deviations at both discharges, suggesting that the dominant sorting mechanism is due to the entrainment potential rather than to preferential depositional processes.

□ Comparison between sampled and virtual patches shows that small scale roughness variations estimated by the local standard deviation of surface elevation at the patch scale are consistent with the variations in the grain size distribution. High-resolution surface topography measurements can be thus used to identify crest and trough regions, to estimate directly the variation in small scale roughness and indirectly the key grain size parameters controlling transport and frictional drag (d_{50} , d_{84}).

□ In terms of total roughness, while bedform heights provide the dominant contribution, the variation in small scale roughness, *e.g.*, d_{84} , still contributes significantly to the total roughness. Local small scale roughness variation between crest and trough suggests that a realistic model of surface topography must resolve both large scale roughness features consistent with the expected bedforms and small scale roughness characteristics consistent with bedform modulated sorting (varying local d_{84} along the bedforms).

Acknowledgments. This research was supported by the National Center for Earth-surface Dynamics (NCED), a Science and Technology Center funded by NSF under agreement EAR-0120914 as well as by NSF grants EAR-0824084 and EAR-0835789. The experiments performed for this study are the follow up of previous experiments (known as StreamLab06) conducted at the St. Anthony Falls Laboratory as part of an NCED program to examine physical-biological aspects of sediment transport (<http://www.nced.umn.edu>). The authors are thankful to Jeff Marr, Craig Hill, and Sara Johnson for providing help in running the experiments. The authors are also thankful to the editors and reviewers whose suggestions and constructive comments substantially improved our presentation and refined our interpretations. Computer resources were provided by the Minnesota Supercomputing Institute, Digital Technology Center at the University of Minnesota.

References

- Aberle, J., and V. Nikora (2006), Statistical properties of armored gravel bed surfaces, *Water Resour. Res.* **42**, W11414, DOI: 10.1029/2005WR004674.
- ASCE Task Committee on Flow and Transport over Dunes (2002), Flow and transport over dunes, *J. Hydraul. Eng. ASCE* **128**, 8, 726-728, DOI: 10.1061/(ASCE)0733-9429(2002)128:8(726).
- Best, J. (2005), The fluid dynamics of river dunes: A review and some future research directions, *J. Geophys. Res.* **110**, F04S02, DOI: 10.1029/2004JF000218.
- Blom, A. (2008), Different approaches to handling vertical and streamwise sorting in modeling river morphodynamics, *Water Resour. Res.* **44**, W03415, DOI: 10.1029/2006WR005474.
- Blom, A., and G. Parker (2004), Vertical sorting and the morphodynamics of bed form-dominated rivers: A modeling framework, *J. Geophys. Res.* **109**, F02007, DOI: 10.1029/2003JF000069.
- Blom, A., J.S. Ribberink, and H.J. de Vriend (2003), Vertical sorting in bed forms: Flume experiments with a natural and a trimodal sediment mixture, *Water Resour. Res.* **39**, 2, 1025, DOI: 10.1029/2001WR001088.
- Blom, A., J.S. Ribberink, and G. Parker (2008), Vertical sorting and the morphodynamics of bed form-dominated rivers: A sorting evolution model, *J. Geophys. Res.* **113**, F01019, DOI: 10.1029/2006JF000618.
- Buffington, J.M., and D.R. Montgomery (1997), A systematic analysis of eight decades of incipient motion studies, with special reference to gravel-bedded rivers, *Water Resour. Res.* **33**, 8, 1993-2029.
- Buffington, J.M., and D.R. Montgomery (1999), Effects of hydraulic roughness on surface textures of gravel-bed rivers, *Water Resour. Res.* **35**, 11, 3507-3521, DOI: 10.1029/1999WR900138.
- Butler, J.B., S.N. Lane, and J.H. Chandler (2001), Characterization of the structure of river-bed gravels using two-dimensional fractal analysis, *Math. Geol.* **33**, 3, 301-330, DOI: 10.1023/A:1007686206695.
- Castaing, B., Y. Gagne, and E.J. Hopfinger (1990), Velocity probability density-functions of high Reynolds number turbulence, *Physica D* **46**, 2, 177-200, DOI: 10.1016/0167-2789(90)90035-N.
- Coleman, S.E., and B.W. Melville (1994), Bed-form development, *J. Hydraul. Eng. ASCE* **120**, 5, 544-560, DOI: 10.1061/(ASCE)0733-9429(1994)120:5(544).
- Coleman, S.E., V.I. Nikora, S.R. McLean, T.M. Clunie, T. Schlicke, and B.W. Melville (2006), Equilibrium hydrodynamics concept for developing dunes, *Phys. Fluids* **18**, 10, 105104, DOI: 10.1063/1.2358332.
- Jerolmack, D., and D. Mohrig (2005), Interactions between bed forms: Topography, turbulence, and transport, *J. Geophys. Res.* **110**, F02014, DOI: 10.1029/2004JF000126.

- Kleinhans, M.G., A.W.E. Wilbers, A. De Swaaf, and J.H. van den Berg (2002), Sediment supply-limited bedforms in sand-gravel bed rivers, *J. Sediment. Res.* **72**, 5, 629-640, DOI: 10.1306/030702720629.
- Lanzoni, S. (2000), Experiments on bar formation in a straight flume: 2. Graded sediment, *Water Resour. Res.* **36**, 11, 3351-3363, DOI: 10.1029/2000WR900161.
- Lanzoni, S., and M. Tubino (1999), Grain sorting and bar instability, *J. Fluid Mech.* **393**, 149-174, DOI: 10.1017/S0022112099005583.
- Leclair, S.F. (2002), Preservation of cross-strata due to the migration of subaqueous dunes: An experimental investigation, *Sedimentology* **49**, 6, 1157-1180, DOI: 10.1046/j.1365-3091.2002.00482.x.
- McElroy, B., and D. Mohrig (2009), Nature of deformation of sandy bed forms, *J. Geophys. Res.* **114**, F00A04, DOI: 10.1029/2008JF001220.
- Nelson, J.M., S.R. McLean, and S.R. Wolfe (1993), Mean flow and turbulence fields over two-dimensional bed forms, *Water Resour. Res.* **29**, 12, 3935-3953, DOI: 10.1029/93WR01932.
- Nelson, J.M., R.L. Shreve, S.R. McLean, and T.G. Drake (1995), Role of near-bed turbulence structure in bed load transport and bed form mechanics, *Water Resour. Res.* **31**, 8, 2071-2086, DOI: 10.1029/95WR00976.
- Nikora, V., and J. Walsh (2004), Water-worked gravel surfaces: High-order structure functions at the particle scale, *Water Resour. Res.* **40**, W12601, DOI: 10.1029/2004WR003346.
- Nikora, V.I., D.G. Goring, and B.J.F. Biggs (1998), On gravel-bed roughness characterization, *Water Resour. Res.* **34**, 3, 517-527, DOI: 10.1029/97WR02886.
- Nordin, C.F., Jr. (1971), Statistical properties of dune profiles, *Geol. Surv. Prof. Paper* **562**, F, 1-41.
- Paola, C., and L. Borgman (1991), Reconstructing random topography from preserved stratification, *Sedimentology* **38**, 4, 553-565, DOI: 10.1111/j.1365-3091.1991.tb01008.x.
- Powell, D.M. (1998), Patterns and processes of sediment sorting in gravel-bed rivers, *Progr. Phys. Geogr.* **22**, 1, 1-32, DOI: 10.1177/030913339802200101.
- Schmeeckle, M.W., and J.M. Nelson (2003), Direct simulation of bedload transport using a local, dynamic boundary condition, *Sedimentology* **50**, 2, 279-301, DOI: 10.1046/j.1365-3091.2003.00555.x.
- Simons, D.B., E.V. Richardson, and C.F. Nordin Jr. (1965), Bedload equation for ripples and dunes, *Geol. Surv. Prof. Pap.* **462**, H, 1-9.
- Singh, A., and E. Foufoula-Georgiou (2012), On the interaction of bed topography, instantaneous shear stress and sediment flux in an experimental channel, **In:** J. Venditti, J. Best, M. Church, and R. Hardy (eds.) *Coherent Flow Structures in Geophysical Flows at Earth's Surface*, Wiley-Blackwell (in print).
- Singh, A., K. Fienberg, D.J. Jerolmack, J. Marr, and E. Foufoula-Georgiou (2009), Experimental evidence for statistical scaling and intermittency in sediment

- transport rates, *J. Geophys. Res.* **114**, F01025, DOI: 10.1029/2007JF000963.
- Singh, A., F. Porté-Agel, and E. Fofoula-Georgiou (2010), On the influence of gravel bed dynamics on velocity power spectra, *Water Resour. Res.* **46**, W04509, DOI: 10.1029/2009WR008190.
- Singh, A., S. Lanzoni, P.R. Wilcock, and E. Fofoula-Georgiou (2011), Multiscale statistical characterization of migrating bed forms in gravel and sand bed rivers, *Water Resour. Res.* **47**, W12526, DOI: 10.1029/2010WR010122.
- Singh, A., E. Fofoula-Georgiou, F. Porté-Agel, and P.R. Wilcock (2012a), Coupled dynamics of the co-evolution of gravel bed topography, flow turbulence and sediment transport in an experimental channel, *J. Geophys. Res.*, DOI: 10.1029/2011JF002323 (in print).
- Singh, A., J.A. Czuba, J. Marr, C. Hill, S. Johnson, C. Ellis, J. Mullin, C.H. Orr, P.R. Wilcock, M. Hondzo, C. Paola, and E. Fofoula-Georgiou (2012b), StreamLab experiments and research synthesis, *Water Resour. Res.*, DOI: 10.1029/2012WR012124 (in print).
- Sumer, B.M., L.H.C. Chua, N.-S. Cheng, and J. Fredsøe (2003), Influence of turbulence on bed load sediment transport, *J. Hydraul. Eng. ASCE* **129**, 8, 585-596, DOI: 10.1061/(ASCE)0733-9429(2003)129:8(585).
- van der Mark, C.F., A. Blom, and S.J.M.H. Hulscher (2008), Quantification of variability in bedform geometry, *J. Geophys. Res.* **113**, F03020, DOI: 10.1029/2007JF000940.
- Venditti, J.G. (2007), Turbulent flow and drag over fixed two- and three-dimensional dunes, *Water Resour. Res.* **112**, F04008, DOI: 10.1029/2006JF000650.
- Venditti, J.G., M.A. Church, and S.J. Bennett (2005), Morphodynamics of small-scale superimposed sand waves over migrating dune bed forms, *Water Resour. Res.* **41**, W10423, DOI: 10.1029/2004WR003461.
- Venugopal, V., S.G. Roux, E. Fofoula-Georgiou, and A. Arneodo (2006), Revisiting multifractality of high-resolution temporal rainfall using a wavelet-based formalism, *Water Resour. Res.* **42**, W06D14, DOI: 10.1029/2005WR004489.
- Wiberg, P.L., and J.M. Nelson (1992), Unidirectional flow over asymmetric and symmetric ripples, *J. Geophys. Res.* **97**, C8, 12745-12761, DOI: 10.1029/92JC01228.
- Wilcock, P.R. (1998), Two-fraction model of initial sediment motion in gravel-bed rivers, *Science* **280**, 5362, 410-412, DOI: 10.1126/science.280.5362.410.
- Yarnell, S.M., J.F. Mount, and E.W. Larsen (2006), The Influence of relative sediment supply on riverine habitat heterogeneity, *Geomorphology* **80**, 310-324, DOI: 10.1016/j.geomorph.2006.03.005.

Received 5 September 2012

Received in revised form 13 September 2012

Accepted 23 September 2012